RSC Advances

PAPER

View Article Online
View Journal | View Issue

Cite this: *RSC Adv.*, 2024, **14**, 36063

Porous, environment-friendly chitosan-ZIF composite fibers for dye adsorption†

Xuebin Hou,[abc] Wei Chen,[a] Meihong Fan[abc] and Chen Shi*[a]

Received 24th September 2024
Accepted 22nd October 2024

DOI: 10.1039/d4ra06883a

rsc.li/rsc-advances

Chitosan (CS) is regarded as a promising sorbent due to its biodegradability, wide availability, easy processing, and multiple active groups. In this work, CS-based porous fibers (ZIF-*n*@CS) consisting of CS and zeolitic imidazolate frameworks (ZIFs) were fabricated through wet spinning and self-assembly methods. This combination effectively utilizes the dual advantages of CS and ZIFs, which effectively remove dyes from water and exhibit excellent recyclability. In addition, the adsorption mechanism of the adsorbent was explored through the analysis of adsorption kinetics, thermodynamics, isotherms, and chemical characterization after adsorption. This work provides an operable and universal strategy for the efficient adsorption of dyes, promoting the further promotion and application of MOFs and CS materials.

1. Introduction

Congo red (CR) and malachite green (MG) are two commonly used synthetic dyes. Classified as a diazo dye, CR contains two azo chromophore groups and four auxochromic groups (amino and sodium sulfonate). It is recognized as a persistent organic pollutant, posing health risks such as poisoning or cancer if individuals are exposed to or consume it over a prolonged period.[1] MG, a derivative of triphenylmethane, is applied in textile printing and dyeing. MG is also employed in fisheries to promote wound healing in fish and prevent bacterial growth. However, studies have shown that MG has teratogenic effects, resulting in delayed hatching and abnormal development of fish eggs.[2] Furthermore, MG and its metabolites can bind with DNA in the human body, potentially leading to cellular cancer.[3,4] Consequently, it is necessary to effectively purify sewage containing these synthetic dyes.

The use of adsorption methods for removing dyes and heavy metal ions in wastewater offers technical advantages, including high efficiency, simple operation, and low cost.[5–7] Compared to other treatment methods such as membrane filtration and flocculation, adsorption poses a lower risk of secondary pollution; therefore, numerous sorbents have been developed for various desired environments.[8] Among these sorbents, naturally degradable polysaccharide polymers (such as chitosan, cellulose, and lignin) have been explored as effective adsorbents for organic synthetic dyes. Chitosan (CS) is regarded as a practical sorbent due to its wide availability, easy processing, multiple active groups, and high adsorption capacity.[9] Current research primarily focuses on modifying substrates or combining them with other nanomaterials of high porosity to achieve efficient adsorption of individual pollutants.[10–12] However, due to economic considerations and the wide range of pollutants present, single-function adsorbents are no longer sufficient to meet the current demands of wastewater treatment. Therefore, combining CS with other materials is a potential strategy to fabricate a multi-functional adsorbent.[13,14]

Metal–organic frameworks (MOFs) are porous materials created by linking metal ions and organic ligands through coordination bonds. They offer benefits such as high porosity, specific surface area, adjustable structure, and easy functionalization.[15–17] In recent years, the application of metal–organic framework (MOFs) materials in air and water filtration has garnered significant attention from researchers. The adsorbent materials derived from MOFs exhibit a high specific surface area,[18] excellent chemical stability, and a distinctive porous structure, all of which contribute to their exceptional adsorption properties. As a typical series of MOFs, zeolitic imidazolate frameworks (ZIFs) have been reported to exhibit a good adsorption property in some published works.[19] However, due to their granular form, ZIFs pose challenges in terms of recycling and reusability, thereby hindering their further development and application. Fibers have emerged as prominent substrates for carrying particulate matter in research due to their elongated shape, high specific surface area, and flexibility.

In view of the above consideration, we have successfully combined chitosan with zeolitic imidazolate framework-8 (ZIF-8) nanomaterials using the self-assembly method in this study,

[a]*College of Textile Science and Engineering, Zhejiang Sci-Tech University, Hangzhou, Zhejiang Province 310018, PR China. E-mail: chenshi2021@zstu.edu.cn*

[b]*Zhejiang Sci-Tech University Shengzhou Innovation Research Institute, Shaoxing, Zhejiang Province 310018, PR China*

[c]*Zhejiang Sci-Tech University Tongxiang Innovation Research Institute, Jiaxing, Zhejiang Province 310018, PR China*

† Electronic supplementary information (ESI) available. See DOI: https://doi.org/10.1039/d4ra06883a

to effectively remove dyes from water. The adsorption property of ZIF-8@CS was evaluated, and results indicated that it has great removal performance for dyes and good recyclability. In addition, the natural factors influencing the adsorption capacity and recycling performance of this composite material were investigated. Through the analysis of adsorption kinetics, thermodynamics, isotherms, and other theoretical models, we aim to gain a comprehensive understanding of its adsorption behavior. Additionally, we conducted a thorough characterization of the fibers before and after adsorption using techniques such as XPS and FT-IR. This work provides an applied strategy for the efficient adsorption of dyes and it will promote the further promotion and application of MOFs and CS materials.

2. Experimental section

2.1 Chemicals

Chitosan, 2-methylimidazole ($C_4H_6N_2$, MIM), sodium hydroxide (NaOH) and glacial acetic acid (CH_3COOH) were provided by Shanghai Maclin Biochemical Technology Co., Ltd. Zinc nitrate hexahydrate ($Zn(NO_3)_2 \cdot 6H_2O$) and cobalt nitrate hexahydrate ($Co(NO_3)_2 \cdot 6H_2O$) were purchased from Shanghai Aladdin Biochemical Technology Co., Ltd. Anhydrous sodium sulfate (Na_2SO_4), glutaraldehyde ($C_5H_8O_2$), calcium chloride ($CaCl_2$), diammonium hydrogen phosphate ($(NH_4)_2HPO_4$), sodium hexametaphosphate $(NaPO_3)_6$, ammonia ($NH_3 \cdot H_2O$), carbinol, and deionized water were obtained from Hangzhou Mick Chemical Instrument Co., Ltd. All dyes including tartrazine (TAR), methylene blue (MB), sunset yellow (SY), crystal violet (CV) and Congo red (CR) were purchased from Shanghai Aladdin Biochemical Technology Co., Ltd. All chemicals were of analytic grade and used without further purification.

2.2 Preparation of CS

Chitosan fiber (CS) was prepared using the wet spinning method according to our previous reports.[20] Chitosan powder was added to a pre-prepared 4% (V/V) acetic acid solution to create a 4% chitosan spinning stock solution. This spinning stock solution was vacuumed and allowed to stand for 24 h before being transferred to a metering pump and extruded into a solidification bath using a syringe pinhole. The coagulation bath was prepared by mixing equal parts of 0.5mol L^{-1} sodium hydroxide solution and 0.1mol L^{-1} anhydrous sodium sulfate solution. The chitosan fiber was cross-linked with glutaraldehyde followed by solidification and washing thoroughly with deionized water until the wash liquid became neutral.

2.3 Preparation of ZIF-*n*@CS composite fibers

Firstly, 30 g of CS fiber was immersed in 200 mL of the 0.1mol L^{-1} zinc nitrate solution, leading to a complex reaction and crosslinking between Zn^{2+} with $-NH_3$ and OH groups of chitosan, and this reaction lasted for 30 minutes. The fiber was then immersed in 200 mL of the 0.4 mol L^{-1} 2-methylimidazole ligand solution for 24 h. After washing with methanol and drying, ZIF-8@CS composite fibers were obtained (as shown in Fig. 1). Additionally, the methods for zeolitic imidazolate framework-67 (ZIF-67)@CS and Zn–Co-ZIF@CS composite fiber were similar except that the zinc nitrate solution was replaced by cobalt nitrate solution and the mixed solution of cobalt nitrate and zinc nitrate, respectively. This self-assembly synthesis method effectively circumvents the influence of a coagulation bath on the chitosan fiber synthesis. Furthermore, compared to the traditional *in situ* growth process, the stability of nano-ZIF_S on the fiber was enhanced.

2.4 Characterization of ZIF-*n*@CS fibrous membranes

The micromorphologies, composition and structure were analyzed using a scanning electron microscope (SEM, Zeiss UItra55), energy dispersive spectrometer (EDS), transmission electron microscope (TEM) and X-ray diffractometer (XRD, Bruker AXS, Cu Kα radiation). Fourier-transformed infrared (FT-IR) and X-ray photoelectron spectrometers (XPS) were applied to analyze the surface chemical states. The porosity and pore volume were measured using the ASAP2020 HD88 nitrogen adsorption–desorption system.

2.5 Removal of dyestuff

In this study, the dye concentration was maintained at 30 ppm. The dye concentration after adsorption was tested by ultraviolet-visible spectroscopy (UV-vis). The ratio between the amount of the adsorbent and the volume of dye solution in the batch adsorption experiment was set at $M_{adsorbent} : V_{dye} = 0.6$ mg mL^{-1}, unless stated otherwise. The calculation of the removal efficiency R_e (%) and adsorption capacity Q_e (mg g^{-1}) was performed using the formulas (3-1) and (3-2):

$$R_e(\%) = \frac{C_0 - C_e}{C_0} \times 100 \quad (3\text{-}1)$$

$$Q_e = \frac{(C_0 - C_{e,t}) \times V}{M} \quad (3\text{-}2)$$

C_0 (mg L^{-1}) and represents the initial concentration of the dye solution, C_e (mg L^{-1}) and C_t(mg L^{-1}) represent the concentration at the adsorption equilibrium and at a certain moment, respectively.

For cyclic adsorption-regeneration experiments, following the dye adsorption experiment, the adsorbent was successfully regenerated through multiple washings with DMF. The ratio of the adsorbent to DMF washing solution was maintained at 0.3 mg mL^{-1}. The washing procedure took place on a constant temperature shaking bed for a duration of 5 h, and the washing was repeated three times until the washing liquid became colorless. Subsequently, the adsorption experiment was resumed.

For selectivity adsorption experiments, the binary mixed dye solution was pre-configured, the concentration of a single component in the mixed dye solution was controlled to be 30 mg L^{-1}, and the adsorption experiment was carried out on the shaking table at 25 °C after adding an appropriate amount of the adsorbent. After the adsorption equilibrium, the dye concentration tests were performed using UV-vis.

Fig. 1 Schematic illustration of the preparation of ZIF-*n*@CS composite fibers.

3. Results and discussion

The infrared spectra of the three types of ZIF materials are depicted in Fig. S1a,† showcasing the prominent stretching vibration of imidazole rings. ZIF-8, ZIF-67, and ZIF-67-8 display closely similar absorption peak spectra. In ZIF-8 and ZIF-67, the absorption peaks at 424 cm^{-1} and 422 cm^{-1} correspond to the stretching vibrations of the Zn–N bond and Co–N bond, respectively. The bimetallic Zn–Co-ZIF sample also shows the stretching vibration of the Zn–N bond and Co–N bond at the same position, indicating that the coordination mode of metal ions and ligands in bimetallic ZIF is consistent with that of monometallic ZIF. Additionally, the vibration peaks at 1583 cm^{-1} is attributed to the stretching vibrations of the C=N bond the imidazole ring in the ligand 2-methylimidazole, the peaks at 2929 cm^{-1} and 3135 cm^{-1} are attributed to the stretching vibrations of the C–H bond on the imidazole ring in the ligand 2-methylimidazole. XRD tests were performed on the three types of ZIFs to further confirm the successful synthesis of ZIF-8, ZIF-67, and ZIF-67-8 (as shown in Fig. S1b†). The results reveal that the characteristic crystal faces of the ZIF materials are consistent, with diffraction peaks aligning closely with the standard sample card (JCPDS 00-062-1030), indicating a comprehensive crystal structure, higher purity, and increased crystallinity compared to that of CS.

SEM images of ZIF-8@CS, ZIF-67@CS, and Zn–Co-ZIF@CS composite fibers correspond to (a), (b), and (c) in Fig. 2, respectively. The images reveal the distinctive 12-hedral structures characteristic of zinc-based and cobalt-based ZIF materials, indicating the successful synthesis of these materials.[21] Furthermore, the SEM images show that ZIF particles were self-assembled onto the chitosan fibers. Fig. 2d presents the mapping image of bimetallic Zn–Co-ZIF nanoparticles on the Zn–Co-ZIF@CS, demonstrating accurate detection of the major metal ions, Zn and Co, and their elemental distribution. This confirms the successful synthesis of the bimetallic ZIF material ZIF-678 (Zn : Co = 1 : 1).

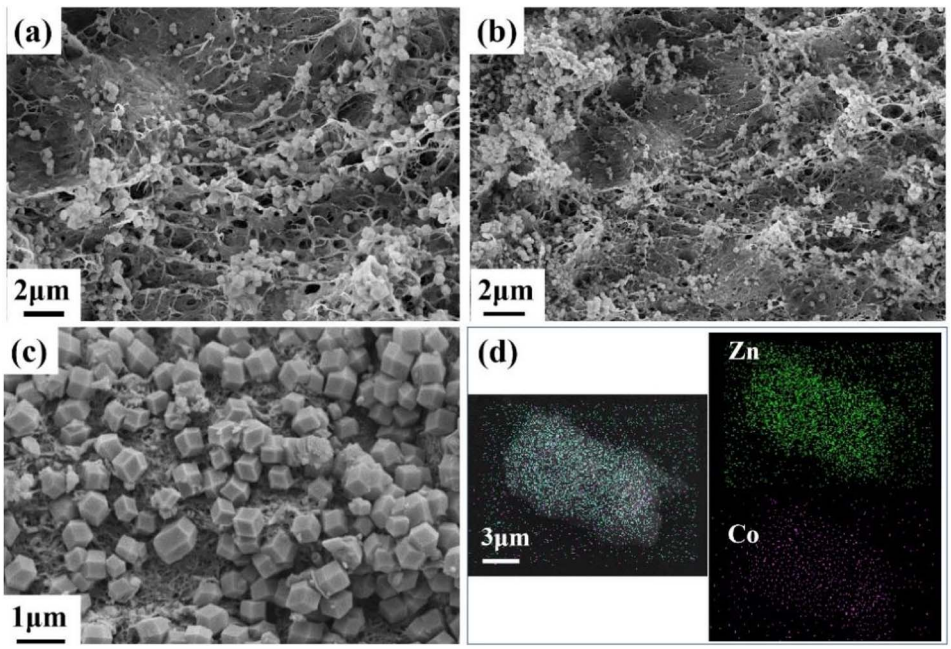

Fig. 2 SEM images of ZIF-8@CS (a), ZIF-67@CS (b) and Zn–Co-ZIF@CS (c), and SEM mapping images of Zn–Co-ZIF@CS (d).

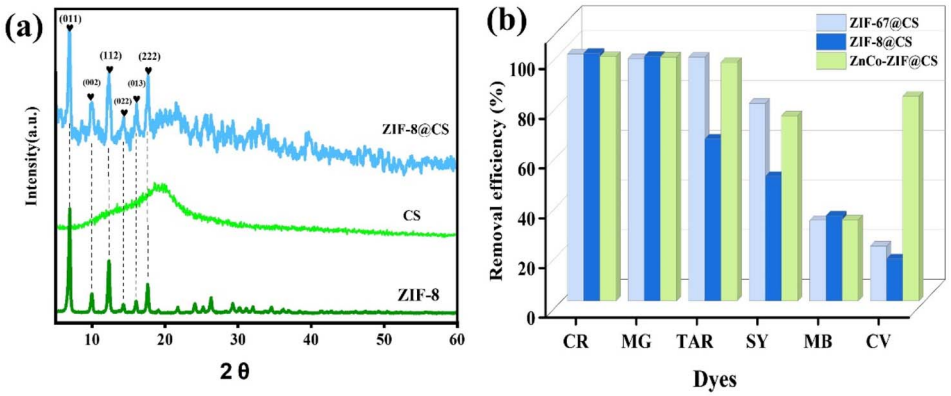

Fig. 3 (a) XRD patterns of ZIF-8, CS and ZIF-8@CS and (b) comparison of adsorption properties of ZIF-67@CS, ZIF-8@CS and Zn–Co-ZIF@CS composite fibers adsorbents for different dyes.

Fig. 3 displays the XRD patterns and adsorption properties of ZIF-8, CS, and ZIF-8@CS fibers towards different dyes. The diffraction peaks observed in ZIF-8@CS composite fiber samples were located at 7.3°, 10.3°, 12.7°, 14.6°, 16.4°, and 17.9°, corresponding to the (011), (002), (112), (022), (013), and (222) crystal planes, respectively, as documented in previous studies.[22–24] This observation confirms the successful synthesis of ZIF-8 on the CS fiber matrix, with the crystal structure of ZIF-8 remaining unchanged throughout the self-assembly growth process. Comparative experiments were conducted on the adsorption of ZIF-8@CS, ZIF-67@CS, and Zn–Co-ZIF@CS fibers with various dyes, as illustrated in Fig. 3b. Overall, the adsorption efficiency of the three fibers for MG and CR dyes surpassed that of other dyes, with ZIF-8@CS exhibiting the most effective dye removal between the three composite fibers. Compared with pure CS fibers (Fig. S6†), the adsorption efficiency of MOFs-*n*@CS composite fibers was obviously improved. It illustrates that MOFs plays a key role in the adsorption of dyes. In consideration of the better stability of the ZIF-8 in an aqueous environment,[25] further investigations were focused on the adsorption behavior of ZIF-8@CS towards MG and CR dyes.

The adsorption efficiency of an adsorbent is influenced by the concentration of the adsorbate.[25] Generally, the adsorption capacity of the adsorbent is fixed, but under too high or low-concentration conditions, this capacity may not be fully utilized. At low concentrations, the likelihood of contact between the adsorbent and adsorbate decreases, making it challenging for the adsorbate to be completely removed from the solution even if there are sufficient adsorption sites. Conversely, the adsorbate molecules tend to aggregate in high-concentration environments, leading to rapid occupation of the adsorbent surface and blockage of adsorption channels, thus diminishing the adsorption capacity of the adsorbent.

Therefore, the removal efficiency of ZIF-8@CS for dye solutions with varying concentrations was evaluated (Fig. 4). The results illustrated a gradual decrease in removal efficiency as the concentration of the dye solution increased. This phenomenon can be attributed to the distribution of dye molecules as monomers in low-concentration environments, allowing for

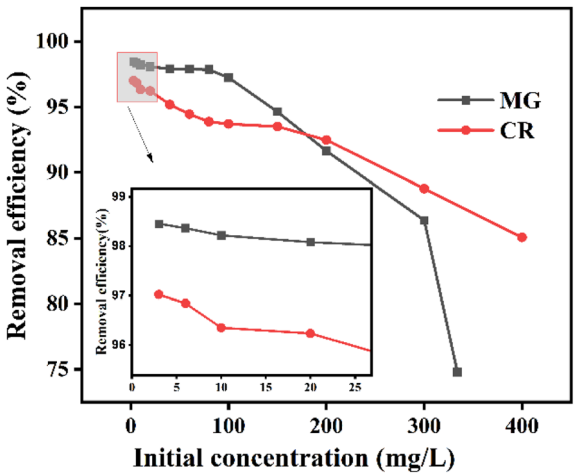

Fig. 4 The removal rate curves of ZIF-8@CS for different initial concentrations of MG and CR dye solutions.

effective contact with adsorption sites and leading to higher removal efficiency. Conversely, in high-concentration environments, adsorption sites become saturated with dye molecules, resulting in diminished post-equilibrium removal efficiency. The optimal performance of ZIF-8@CS composite fiber was observed when the dye concentration did not exceed 100 mg L^{-1}. Furthermore, distinct differences were noted in the adsorption behavior of ZIF-8@CS composite fiber towards the two dyes. Specifically, at low concentrations, the removal rate of MG surpassed that of CR, possibly due to the smaller molecular size of MG. While at high concentrations, the removal rate of CR exceeded that of MG, potentially due to stronger stacking interactions among the MG molecules. Experimental results indicated adsorption capacities of 568.47 mg g^{-1} for CR and 412.75 mg L^{-1} for MG.

For a specific concentration of the dye liquor, there exists an optimal amount of adsorbent that matches it. This ideal ratio of the adsorbent to dye liquor maximizes the efficiency of the adsorbent.[26] Excessive use of the adsorbent in an environment with a certain dye liquor concentration can lead to economic

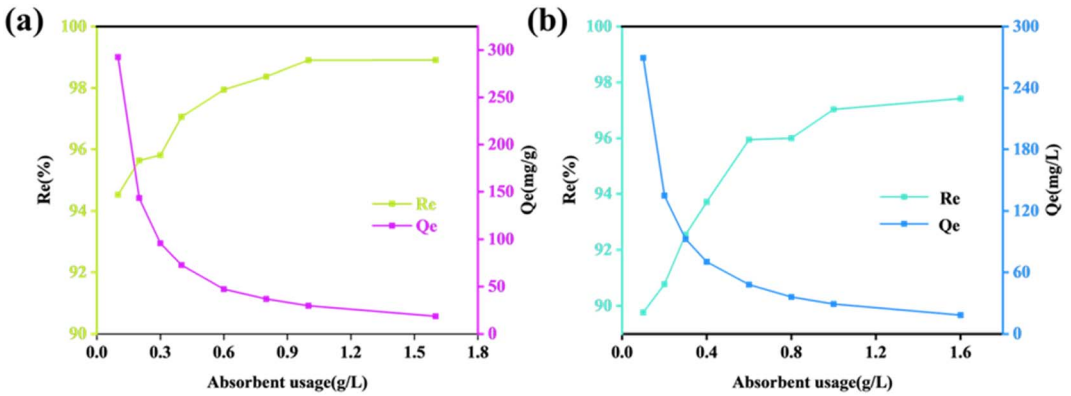

Fig. 5 Removal efficiency curves of CR (a) and MG (b) dyes with different adsorbent ZIF-8@CS dosages (R_e: removal efficiency; Q_e: adsorption capacity).

waste and suboptimal utilization of the adsorbent. Consequently, exploratory experiments were carried out. Fig. 5 illustrates that the ZIF-8@CS composite fiber's adsorption of the two dyes (CR and MG) follows a similar process, where the removal efficiency R_e gradually increases with the amount of the adsorbent, while the unit adsorption capacity Q_e subsequently decreases due to the provision of adequate adsorption sites by the optimal amount of the adsorbent. The experiment concluded that for dye liquor concentrations <100 ppm, an adsorbent dosage of 0.6 g L^{-1} can guarantee a removal rate exceeding 96% and achieve the highest level of adsorbent utilization efficiency.

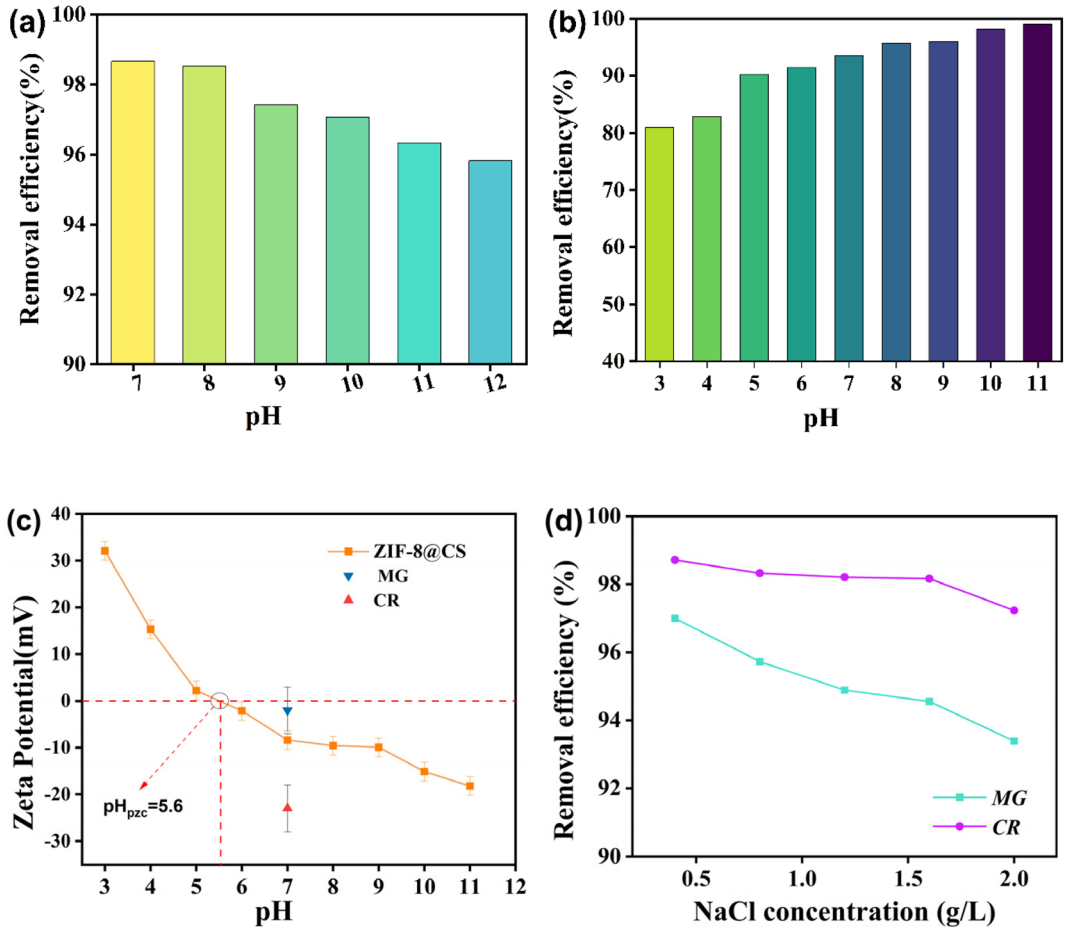

Fig. 6 (a and b) Removal efficiency of ZIF-8@CS for CR (a) and MG (b) at different pH values (c) ZETA potential of ZIF-8@CS at different pH values and (d) removal efficiency of ZIF-8@CS for CR and MG at different contents of sodium chloride.

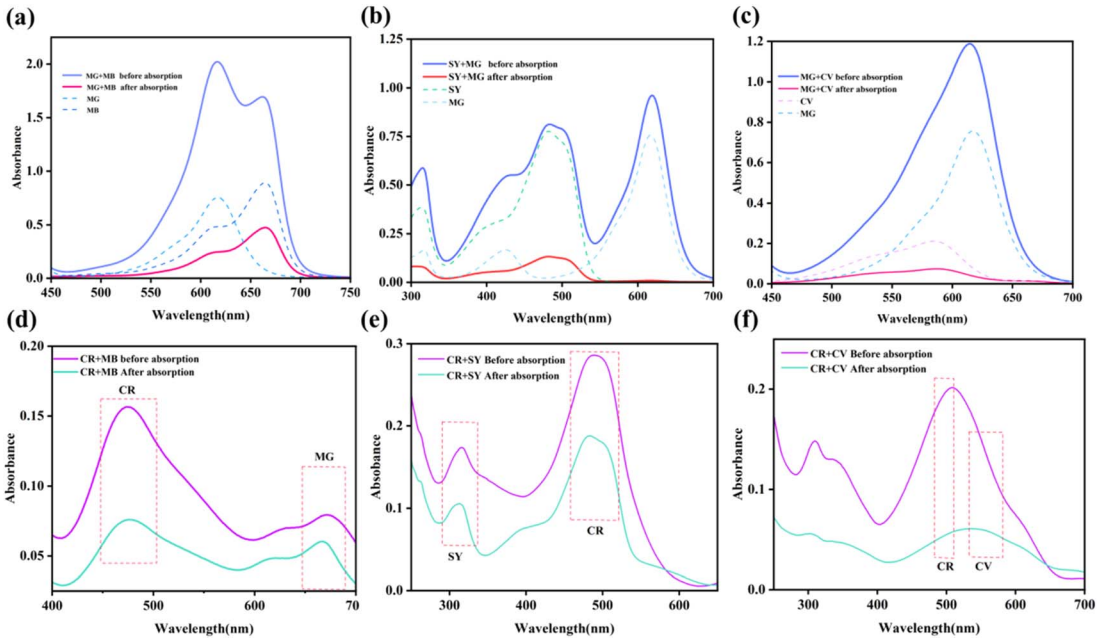

Fig. 7 UV-vis curves before and after the adsorption process in a binary mixed dye solution system (a) MG + MB system; (b) SY + MG system; (c) MG + CV system; (d) CR + MB system (e) CR + SY system; (f) CR + CV system.

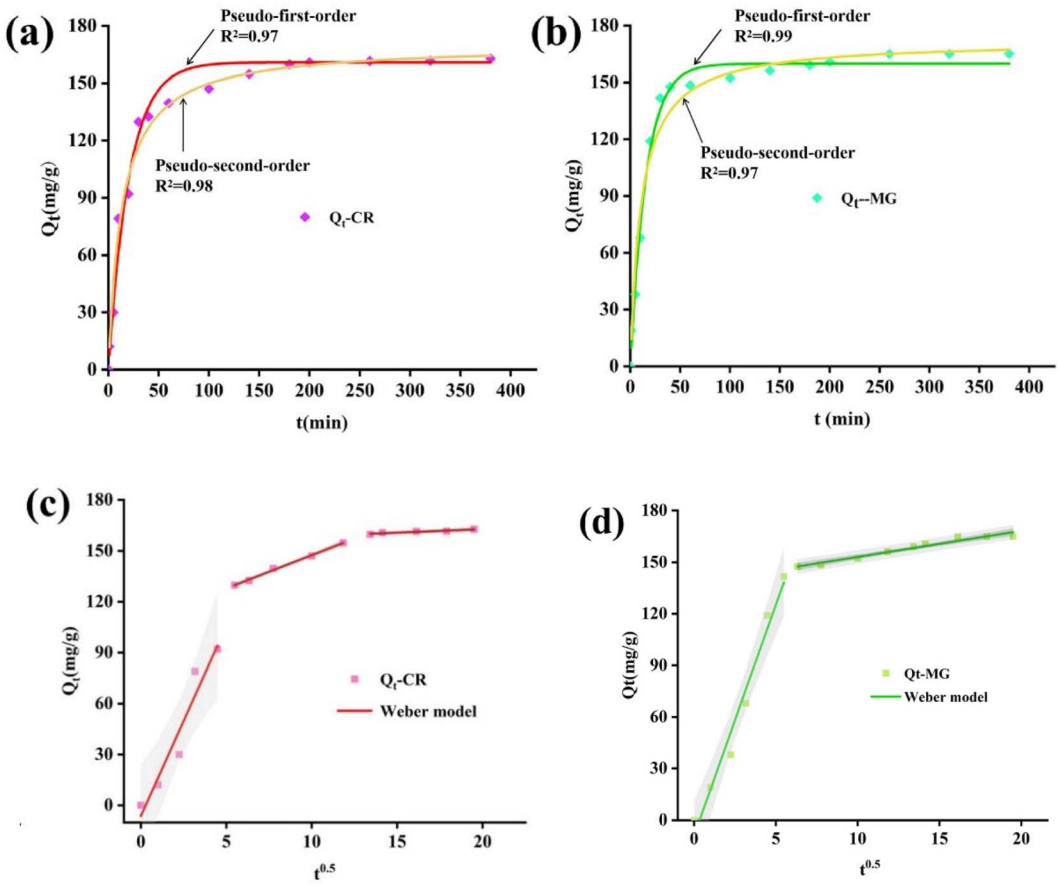

Fig. 8 (a and b) Pseudo-first-order kinetics and pseudo-second-order kinetics plots CR and MG adsorption on composite fibers; (c and d) Weber–Morris model kinetics plots CR and MG adsorption on composite fibers.

Fig. 6a and b illustrates the removal performance of ZIF-8@CS for CR and MG dyes at varying pH levels. The figure demonstrates that the composite fiber's adsorption behavior towards the two dyes exhibits contrasting characteristics in response to changes in pH. Specifically, the adsorption of CR dye shows a decrease in the removal rate with increasing alkalinity, whereas the adsorption of MG displays a decrease in the removal rate with stronger acidity. This trend could be attributed to the potential of the dyes and the protonation of the functional groups on ZIF-8@CS. Specifically, CR and MG dyes exhibit opposite behaviors when dissolved in water due to their different electronegativity. The ZETA potential performance of ZIF-8@CS at various pH levels suggests that the electronegativity of ZIF-8@CS is enhanced in an alkaline environment, leading to electrostatic force repulsion due to the negatively charged CR dye molecules. Conversely, in an acidic environment, the positive charge of ZIF-8@CS increased, resulting in electrostatic attraction toward negatively charged CR. Therefore, the removal rate of CR decreases with higher alkalinity, while the opposite effect is observed for MG.

In environments where dyes are used daily, sodium salts are commonly added to dye solutions as fixing or coloring agents. These sodium salts are often discharged into dye wastewater, becoming a significant factor in dye adsorption. To investigate this, we conducted a single variable comparison experiment. The result shows (illustrated in Fig. 6d) that in an environment with a specific amount of adsorbent and dye solution concentration, the overall dye removal rate decreases as the sodium concentration increases. The impact on MG is more pronounced than on CR, attributed to the ion shielding effect. The presence of sodium salt shields the electrical properties of both the dye and adsorbent, diminishing the electrostatic interaction between them. The disparity in the removal rates between CR and MG could be attributed to the varying strength of this shielding effect. At pH 7, the ZIF-8@CS composite fiber should exhibit electrostatic repulsion towards CR molecules and electrostatic attraction towards MG molecules. However, the presence of sodium salt weakens both the repulsion and attraction. Consequently, CR dye molecules can penetrate deeper into the adsorption site, while MG molecules find it more challenging to enter, resulting in the discrepancy in removal rates between the two.

In the context of printing and dyeing wastewater treatment, adsorbents are exposed to a wide range of pollutants. An important consideration for the practicality and efficiency of adsorbents is whether they can selectively adsorb specific substances from a diverse mixture of pollutants. This is crucial because if adsorbents lack selective adsorption capabilities,

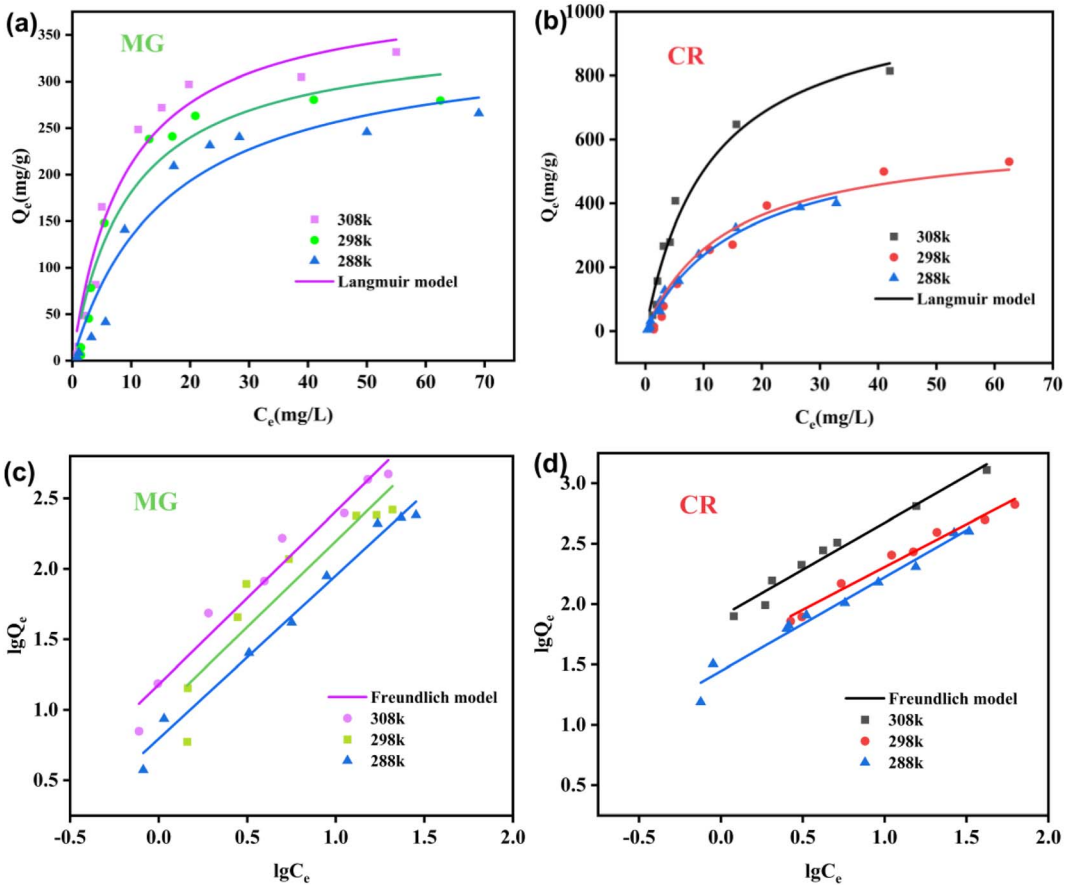

Fig. 9 (a and b) Fitting of the Langmuir model for adsorption isothermal plots of ZIF-8@CS toward MG and CR; (c and d) Freundlich model for adsorption isothermal plots of ZIF-8@CS toward MG and CR.

they would need to possess high adsorption capacity to effectively treat mixed dye solutions. Additionally, the process of dye desorption typically requires a significant amount of elution solvent, making it challenging to reuse the mixed dye solution afterwards. Hence, this study delves into the selective adsorption properties of ZIF-8@CS composite fibers in binary mixed dye scenarios. As depicted in Fig. 7, the ZIF-8@CS composite fiber demonstrates favorable adsorption selectivity in the binary mixed systems of MG + MB, MG + SY, and MG + CV. The selectivity observed in the MG + MB and MG + CV systems may be attributed to factors such as the shape and size of the dye molecules, hydrogen bond energy, and intermolecular interactions. Conversely, in the MG + SY system, the selectivity of the adsorbent is likely influenced by electrostatic forces. The negatively charged ZIF-8@CS composite fibers attract positively charged MG molecules while repelling the negatively charged anionic dye SY. During the adsorption process, these influencing factors may act simultaneously. Furthermore, the result illustrates that the ZIF-8@CS composite fiber does not exhibit selectivity for CR.

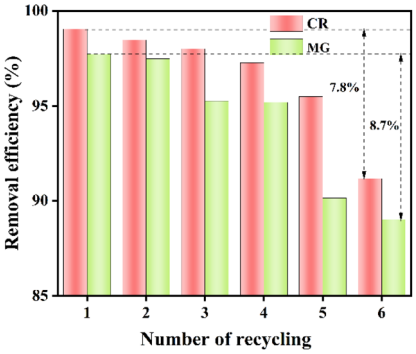

Fig. 10 Antibacterial rate of ZIF-8@CS for CR and MG after different washing times.

The results from Fig. 8 suggest that the experimental data of CR is better fitted with the pseudo-second-order kinetic model. While the pseudo-first-order kinetic model is more suitable for MG adsorption with a fitting degree of 0.99. Besides, the Weber–Morris model was applied for kinetic analysis (shown in Fig. 8c and d), through the analysis of the fitting data, it can be proved

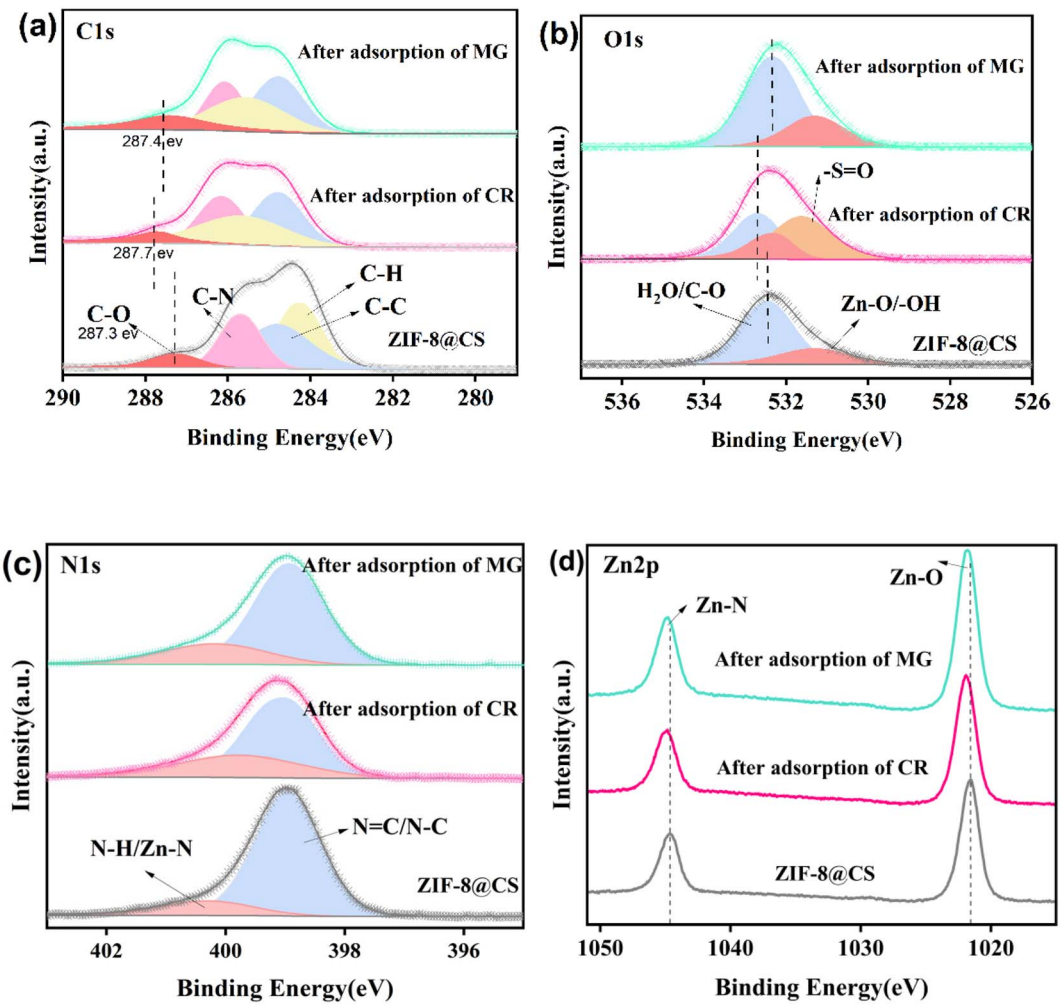

Fig. 11 XPS spectra of ZIF-8@CS before and after CR and MG adsorption (a) high-resolution spectra of C 1s (b) high-resolution spectra of O 1s (c) high-resolution spectra of N 1s and (d) high-resolution spectra of Zn 2p.

that the adsorption process of ZIF-8@CS is controlled by not only a single factor, which indicates that there are other factors affecting the adsorption rates besides the diffusion rate of dye molecules. CR is an anionic dye and in a neutral environment, the adsorption of CR by ZIF-8@CS is mainly due to the formation of chemical bonds with functional groups such as hydroxyl and amino groups on the surface of the adsorbent, which may also include hydrogen bonds, π–π accumulation and van der Waals forces. Electrostatic force does not play a dominant role in this system.[27,28] The adsorption of MG, a cationic dye, and the adsorption rate of ZIF-8@CS on MG is predominantly influenced by the diffusion rate of the dye molecules, and it is consistent with the ZETA potential results. The electrostatic attraction between ZIF-8@CS and MG molecules emerges as the primary factor affecting dye diffusion.

From Fig. 9, it can be concluded that the Langmuir model is more suitable for explaining the CR adsorption process of the ZIF-8@CS composite fiber compared to the MG, suggesting that the adsorption process of ZIF-8@CS for CR follows a point-to-point single-layer uniform adsorption process, while the adsorption process for MG is better explained by the Freundlich model.

The recyclability of the adsorbent is a critical factor in determining its practical applicability. Fig. 10 illustrates that while the removal efficiency gradually decreases with each cycle, it remains above 90% for a 50 mg L^{-1} dye solution even after 6 cycles. The adsorption of ZIF-8@CS on CR and MG shows a slight decrease of 7.8% and 8.7% respectively, suggesting that ZIF-8@CS can be regenerated and reused. The decline in the removal efficiency may be attributed to the type of eluent used and the stability of ZIF-8. When using the organic solvent DMF as an eluent, it may not completely displace all dye molecules, leading to some adsorption sites on the ZIF-8@CS surface remaining occupied during subsequent cycles, thereby causing a reduction in the removal efficiency.

3.1 Adsorption mechanism

To investigate the adsorption mechanism of Congo Red (CR) and Malachite Green (MG) on ZIF-8@CS composite fiber, X-ray photoelectron spectroscopy (XPS) was used to characterize the ZIF-8@CS composite fiber, both, before and after dye adsorption (Fig. 11). The adsorption of CR and MG on ZIF-8@CS resulted in an increase in the binding energy of the C–O bond in the high-resolution C 1s map from 287.3 eV to 287.7 eV and 287.4 eV, respectively (as shown in Fig. 11a). Similar changes in the binding energy were observed in the O 1s high-resolution spectra (Fig. 11b). This suggests a decrease in electron density within the group, indicating the participation of the hydroxyl group in the adsorption reaction and the formation of hydrogen bonds during the process.[29] Additionally, the C–N binding energy increased in both the C 1s and N 1s high-resolution spectra after the adsorption reaction, implying the involvement of the amino group on the adsorbent surface in the adsorption process and the formation of new hydrogen bonds. After the CR adsorption at ZIF-8@CS, a new binding peak at 531.6 eV in the O 1s spectrum corresponding to S=O of CR was observed, suggesting the stable adsorption of CR on ZIF-8@CS. Analysis of the Zn 2p spectrum revealed a slight increase in binding energy for both Zn–N and Zn–O after the adsorption, implying the involvement of ZIF-8 in the process. This could be attributed to the formation of new coordination bonds between Zn and dye molecules or π–π interactions between the imidazole rings and dye molecules.[30]

FT-IR analysis of ZIF-8@CS was conducted pre- and post-dye adsorption to investigate the adsorption mechanism (Fig. S5†). The results revealed a shift towards blue in the hydroxyl peaks at 3382 cm^{-1} after CR and MG adsorption, suggesting the formation of new hydrogen bonds during the process. Additionally, the absorption peak at 420 cm^{-1} attributed to Zn–N stretching vibration exhibited a blue shift post-adsorption, suggesting new coordination was formed. This coordination potentially involves Zn with $–NH_2$ and $–SO_3$ in CR dye molecules or C–N bonds with MG dye molecules.

4. Conclusions

In this study, composite fibers of CS-ZIFs (ZIF-8@CS) were successfully fabricated using wet spinning and self-assembly methods. The composite material exhibited excellent adsorption capabilities for both the anionic dye CR (593 mg g^{-1}) and the cationic dye MG (401 mg g^{-1}), which were significantly higher than those of the individual monomer adsorption materials. When tested in a binary mixed dye solution, ZIF-8@CS showed selectivity for the MG dye. XPS and FT-IR characterization indicated a similar adsorption mechanism for both dyes, involving hydrogen bonding, π–π stacking between the imidazole ring and benzene ring in the dye molecules, coordination between Zn and the dye molecules, as well as electrostatic forces. Moreover, the material retained over 90% of its adsorption capacity after 5 sorption–desorption cycles, demonstrating its potential for practical applications.

Data availability

The data supporting this article are included as part of the ESI.†

Conflicts of interest

There are no conflicts to declare.

Acknowledgements

This research was financially supported by the Baima Lake Laboratory Joint Funds of the Zhejiang Provincial Natural Science Foundation of China under Grant (No. LBMHZ24B060005), Foundation of Zhejiang Sci-Tech University Shengzhou Innovation Research Institute (No. SYY2024C000009). Foundation of Zhejiang Sci-Tech University Tongxiang Innovation Research Institute (No. TYY202401). Advanced Fiber Materials Engineering Research Center of Anhui Province (No. 2023AFMC13).

References

1 T. Yuqi, X. Zhang, X. Li, *et al.*, Facile synthesis of magnetic ZnAl layered double hydroxides and efficient adsorption of malachite green and Congo red, *Separ. Purif. Technol.*, 2023, **322**, 124305.

2 A. C. Harry, M. John, M. Paul, *et al.*, Brewers' spent grain in adsorption of aqueous Congo Red and malachite Green dyes: Batch and continuous flow systems, *J. Hazard. Mater.*, 2019, **380**, 120897.

3 W. Miao, Z. Jie, Z. Meng, *et al.*, Facile fabrication of bioinspired hierarchical porous MOFs for selective adsorption of Congo red and Malachite green from vegetables and fruits juices, *Environ. Technol. Innovat.*, 2023, **30**, 103132.

4 C. Frank, M. Julia, P. Anjoeka, *et al.*, Carcinogenicity of gentian violet, leucogentian violet, malachite green, leucomalachite green, and CI Direct Blue 218, *Lancet Oncol.*, 2021, **22**(5), 585–586.

5 M. Shabir, M. Yasin, M. Hussain, *et al.*, A review on recent advances in the treatment of dye-polluted wastewater, *J. Ind. Eng. Chem.*, 2022, **112**, 1–19.

6 H. M. Solayman, Md A. Hossen, A. Abd Aziz, *et al.*, Performance evaluation of dye wastewater treatment technologies: A review, *J. Environ. Chem. Eng.*, 2023, **11**(3), 109610.

7 C. X. H. Su, L. W. Low, T. T. Teng, *et al.*, Combination and hybridisation of treatments in dye wastewater treatment: A review, *J. Environ. Chem. Eng.*, 2016, **4**(3), 3618–3631.

8 J. El-Gaayda, F. E. Titchou, R. Oukhrib, *et al.*, Natural flocculants for the treatment of wastewaters containing dyes or heavy metals: A state-of-the-art review, *J. Environ. Chem. Eng.*, 2021, **9**(5), 106060.

9 Z. Wen, R. Peng, D. Gao, *et al.*, Chitosan-alginate sponge with multiple cross-linking networks for adsorption of anionic dyes: Preparation, property evaluation, mechanism exploration, and application, *J. Chromatogr. A*, 2024, **1713**, 464507.

10 Y. Zhang, B. Mei, B. Shen, *et al.*, Preparation of biochar@chitosan-polyethyleneimine for the efficient removal of uranium from water environment, *Carbohydr. Polym.*, 2023, **312**, 120834.

11 Y. Gao, P. Cai, L. Zhong, *et al.*, Chitosan-polyvinyl alcohol-diatomite hydrogel removes methylene blue from water, *Int. J. Biol. Macromol.*, 2024, **254**, 127886.

12 W. Wang, H. Bai, Y. Zhao, *et al.*, Synthesis of chitosan cross-linked 3D network-structured hydrogel for methylene blue removal, *Int. J. Biol. Macromol.*, 2019, **141**, 98–107.

13 S. Fan, Z. Huang, Y. Zhang, *et al.*, Magnetic chitosan-hydroxyapatite composite microspheres: Preparation, characterization, and application for the adsorption of phenolic substances, *Bioresour. Technol.*, 2019, **274**, 48–55.

14 R. E. K. Billah, M. A. Khan, Y. K. Park, *et al.*, A Comparative Study on Hexavalent Chromium Adsorption onto Chitosan and Chitosan-Based Composites, *Polymers*, 2021, **13**(19), 3427.

15 J. Lin, W. Ye, M. Xie, *et al.*, Environmental impacts and remediation of dye-containing wastewater, *Nat. Rev. Earth Environ.*, 2023, **4**(11), 785–803.

16 T. Wang, F. Chen, L. Jiang, *et al.*, Metal–Organic-Framework-Derived Bromine and Nitrogen Dual-Doped Porous Carbon for CO_2 Photocycloaddition Reaction, *Inorg. Chem.*, 2024, **63**(9), 4224–4232.

17 X. Hou, K. Xie, Z. Huang, C. Shi, *et al.*, Co-MOF induced "blossom branch like" MoS_2@Co_9S_8/C nanofibers as a bifunctional catalyst for HER and OER, *Appl. Surf. Sci.*, 2023, **616**, 156486.

18 S. Kouser, A. Hezam, M. J. N. Khadri, *et al.*, A review on zeolite imidazole frameworks: synthesis, properties, and applications, *J. Porous Mater.*, 2022, **29**(3), 663–681.

19 Z. Zhe, C. Yi, L. Manni, *et al.*, Tailored design of hierarchically porous metal/N-codoped carbon from soft-templated bimetallic ZIFs for the high-efficiency adsorption of tetracycline hydrochloride, *Sep. Purif. Technol.*, 2024, **333**, 125898.

20 C. Wei, S. Chen, H. Jian, *et al.*, In situ growth ZIF-8 on porous chitosan/hydroxyapatite composite fibers for ultra-efficiently eliminating lead ions in wastewater, *Mater. Today Commun.*, 2023, **37**, 107255.

21 H. N. Abdelhamid, Zeolitic imidazolate frameworks (ZIF-8, ZIF-67, and ZIF-L) for hydrogen production, *Appl. Organomet. Chem.*, 2021, **35**(9), e6319.

22 F. Şahin, B. Topuz, H. Kalıpçılar, *et al.*, Synthesis of ZIF-7, ZIF-8, ZIF-67 and ZIF-L from recycled mother liquors, *Microporous Mesoporous Mater.*, 2018, **261**, 259–267.

23 S. Sadiq, I. Khan, M. Humayun, *et al.*, Synthesis of Metal–Organic Framework-Based ZIF-8@ZIF-67 Nanocomposites for Antibiotic Decomposition and Antibacterial Activities, *ACS Omega*, 2023, **8**(51), 49244–49258.

24 Z. Hu, H. Zhang, X. F. Zhang, *et al.*, Polyethylenimine grafted ZIF-8@cellulose acetate membrane for enhanced gas separation, *J. Membr. Sci.*, 2022, **662**, 120996.

25 S. Nie, F. Chen, K. Chen, *et al.*, Enhancement of CO_2 adsorption and separation in basic ionic liquid/ZIF-8 with core-shell structure, *Chem. Commun.*, 2024, **60**, 3559–3562.

26 C. Hua, Z. Yi, W. Jian, *et al.*, Polydopamine modified cyclodextrin polymer as efficient adsorbent for removing cationic dyes and Cu^{2+}, *J. Hazard. Mater.*, 2020, **389**, 121897.

27 X. Wang, M. Zheng, X. Gang, *et al.*, Synergizing redox of zerovalent iron and singlet oxygen to remove aniline, chromium and antimony in printing and dyeing wastewater synchronously: Multifunctional effect of sludge derived biochar, *Chem. Eng. J.*, 2023, **476**, 146927.

28 J. Li, L. Huang, X. Sun, *et al.*, Preparation and characterization of ternary Cu/Cu_2O/C composite: An extraordinary adsorbent for removing anionic organic dyes from water, *Chem. Eng. J.*, 2021, **404**, 127091.

29 K. Y. A. Lin and H. A. Chang, Ultra-high adsorption capacity of zeolitic imidazole framework-67 (ZIF-67) for removal of malachite green from water, *Chemosphere*, 2015, **139**, 624–631.

30 M. El Youssfi, A. Sifou, R. Ben Aakame, *et al.*, Trace elements in Foodstuffs from the Mediterranean Basin—Occurrence, Risk Assessment, Regulations, and Prevention strategies: A review, *Biol. Trace Elem. Res.*, 2023, **201**(5), 2597–2626.